CRITERIA FOR FLUX ROPE ERUPTION: NON EQUILIBRIUM VERSUS TORUS INSTABILITY

P. DÉMOULIN AND G. AULANIER
LESIA, Observatoire de Paris, CNRS, 5 place Jules Janssen, 92190 Meudon, France
Draft version June 5, 2010

ABSTRACT

The coronal magnetic configuration of an active region typically evolves quietly during few days before becoming suddenly eruptive and launching a coronal mass ejection (CME). The precise origin of the eruption is still debated. Among several mechanisms, it has been proposed that a loss of equilibrium, or an ideal magneto-hydrodynamic (MHD) instability such as the torus instability, could be responsible for the sudden eruptivity. Distinct approaches have also been formulated for limit cases having circular or translation symmetry. We revisit the previous theoretical approaches, setting them in the same analytical framework. The coronal field results from the contribution of a non-neutralized current channel added to a background magnetic field, which in our model is the potential field generated by two photospheric flux concentrations. The evolution on short Alfvénic time scale is governed by ideal MHD. We show analytically first that the loss of equilibrium and the stability analysis are two different views of the same physical mechanism. Second, we identify that the same physics is involved in the instability of circular and straight current channels. Indeed, they are just two particular limiting case of more general current paths. A global instability of the magnetic configuration is present when the current channel is located at a coronal height, h, large enough so that the decay index of the potential field, $\partial \ln |\mathbf{B}_{\mathrm{p}}|/\partial \ln h$ is larger than a critical value. At the limit of very thin current channels, previous analysis found a critical decay index of 1.5 and 1 for circular and straight current channels, respectively. However, with current channels being deformable and as thick as expected in the corona, we show that this critical index has similar values for circular and straight current channels, typically in the range [1.1,1.3].

Subject headings: Sun: corona — Sun: filaments — Sun: flares — Sun:magnetic fields — Sun: photosphere

1. INTRODUCTION

A coronal mass ejections (CME) is the consequence of the sudden destabilization of a part of the coronal magnetic field. The eruption is preceded by a long phase (days to week) during which the magnetic field is progressively stressed and free magnetic energy builds up. The configuration typically grows quasi-statically (with velocities well below the Alfvén velocity). At a point of the evolution, in a few minutes up to an hour, the system becomes very dynamic, with a global upward motion, as traced by the evolution of the cold plasma in the associated filament and of the hot plasma in coronal loops. Later on, a significant release of magnetic energy occurs, and a flare is typically observed. If the downward magnetic tension of the covering magnetic arcade is weak enough, the erupting plasma and magnetic field is launched towards the interplanetary space as a CME. In summary, the CME phenomena occurs in four main phases: build-up, instability, acceleration, and propagation. They have been reviewed by Forbes et al. (2006) and Vršnak (2008).

The two last phases are the most spectacular ones, so they are better constrained by observations and they are more deeply modeled, in particular with MHD simulations (e.g. Amari et al. 2003; Fan & Gibson 2007; Török & Kliem 2007). The first phase is a slow evolution and it is usually difficult to characterize in observations what are the generic key points which lead to eruption. The main physics which emerges from obser-

Electronic address: Pascal.Demoulin@obspm.fr

vations is the presence of new emerging magnetic flux, progressive dispersion of the whole flux, the build up of a very sheared field in the vicinity of the photospheric inversion line (PIL), and the cancelation of flux at the PIL (e.g. van Driel-Gesztelyi 1998; Green et al. 2002; van Driel-Gesztelyi et al. 2003). At the least the three last are physically related since flux dispersion lead to the convergent flows towards the PIL, increasing the magnetic shear and forcing flux cancelation. This also implies the build-up of a flux rope with J-shaped coronal loops transformed by reconnection into S-shaped loops (e.g. Moore et al. 1995; Gibson et al. 2006; Green & Kliem 2009).

A still open issue is why does the magnetic configuration erupt? There is usually no evidence of a large amount of new magnetic flux (with a magnitude comparable to the pre-eruptive flux), so the eruption is not driven by the sub-photospheric evolution but rather the coronal magnetic configuration becomes unstable at some point during the slow evolution. During this phase, magnetic reconnection is probably involved as a key mechanism for the progressive transformation of the magnetic configuration. However, an ideal instability is thought to initiate the CME since the upward acceleration phase starts before the impulsive phase of the flare in the majority of events (e.g. Kahler et al. 1988; Maričić et al. 2007). Later on, magnetic reconnection plays a key role in the eruption as the peak of the upward acceleration is typically found correlated with the peak of the hard X-rays and of the time derivative of soft X-rays flux (e.g. Neupert et al. 2001; Zhang et al. 2001; Vršnak et al. 2004; Temmer et al. 2008).
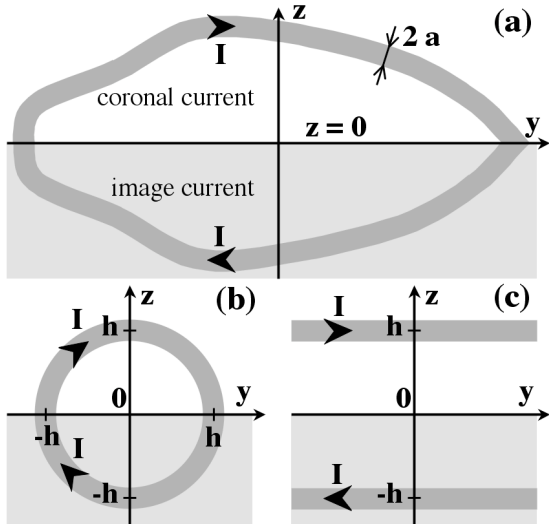
FIG. 1.— **(a)** Schema of a current channel in the corona and its image current below the photosphere (located at $z = 0$). The current channel has a radius a. **(b,c)** Particular cases with a circular and straight current channels, respectively.

Magnetic reconnection also plays a key role during the first phase as it permits the progressive transformation of very sheared field lines into a twisted flux rope. However, the MHD simulations of Aulanier et al. (2010) have shown that magnetic reconnection at the photospheric level, or later on in the corona below the flux rope, is not directly responsible for the onset of the eruption. The configuration rather gets unstable when the flux rope reaches a height where the potential field, associated to the distribution of the photospheric magnetic flux, is decreasing fast enough with height. This relates the onset of the eruption in MHD simulations to a series of analytical studies, as summarized below.

The equilibrium of a flux rope within a coronal field was first considered by Kuperus & Raadu (1974) with the following simplifications. In Cartesian coordinates, they modeled a flux rope with the magnetic field created by a straight line current of intensity I, located at a height, $z = h$, above the photosphere located at $z = 0$ (Figure 1(c)). The flux rope field is added to a simple background magnetic field: a potential field, $\mathbf{B}_p$, associated to a bipolar photospheric magnetic field. They included the observed insignificant evolution of the vertical component, B_z, at the photospheric level during the instability phase of a CME by introducing an image current of intensity $-I$, located at the height $z = -h$. The physical result is that two oppositely directed Laplace forces are acting on the coronal line current: one from the potential field, $\mathbf{B}_p$, and the other from the magnetic field created from the image current (or the equivalent surface current at $z = 0$). The equilibrium is then described by a curve $I(h)$.

van Tend & Kuperus (1978) showed that, $I(h)$ is an increasing function of h at low height and that it has a local maximum if the horizontal component of $\mathbf{B}_p$ orthogonal to the line current, $|B_{p,x}|$, decreases fast enough with height. Then, supposing that the current I can be increased progressively to larger values during the buildup phase, a loss of equilibrium occurs at $h = h_{\mathrm{crit.}}$ defined by the maximum of the function $I(h)$. This occurs where $|B_{p,x}|$ decreases faster than $1/h$. This model was later

developed within a circuit theory, introducing an electric potential and a resistance in the circuit to describe the temporal evolution of I. The current sheet which forms below the erupting flux rope was described by another electric circuit. This provides a set of coupled equations which describes the main phases of an eruptive flare (Martens & Kuin 1989; van Ballegooijen & Martens 1989). Next, the background potential field, $\mathbf{B}_p$, was replaced by a linear force-free field to include, as observed, a sheared field (Amari & Aly 1989). A loss of of equilibrium is also present if $|B_{p,x}|$ is decreasing fast enough with height (Démoulin & Priest 1988).

In the above theory, it is supposed that the current intensity, I, is the main driver of the evolution and that it can be increased to arbitrary large values. However, the coronal physics is not precisely described by any circuit theory because the electric current is a consequence of the force balance together with MHD constraints (e.g. Parker 1996a). The effect of magnetic reconnection on the system (through changing field line connectivity and energy release) before the flare/CME acceleration phase is minimal and therefore the stability of an equilibrium is typically tested in ideal MHD. The conservation of the coronal magnetic flux passing below the flux rope is typically used to set a constraint on the current evolution. Anzer & Ballester (1990) claimed that there is no longer a loss of equilibrium with this ideal MHD constraint, but Démoulin et al. (1991) found that this constraint mostly displaced the loss of equilibrium point to a larger height (slightly after the maximum of the $I(h)$ curve), in agreement with the MHD simulation of Forbes (2000). The following developments have shown that a loss of equilibrium is typically present if the flux rope radius is thin enough. It occurs, for example, when the photospheric polarities are subject to converging motions toward the PIL, or when their magnetic flux is decreased, even when ideal MHD is assumed during the full build-up phase, (Isenberg et al. 1993; Forbes & Isenberg 1991; Forbes & Priest 1995).

When the current channel is curved, an extra force is present, called the hoop force (e.g. Bateman 1978). The electric current of a curved channel creates a magnetic field component orthogonal to the channel. This implies an outward Laplace force (away from the curvature center). In terms of the magnetic field, this force is due to the over magnetic pressure of the azimuthal field component present in the direction of the curvature center. This force is at the heart of the magnetically driven model of Chen (1989) and subsequent developments (e.g. Garren & Chen 1994; Krall et al. 2000). This force is also present in MHD models where the straight line current of previous paragraph is replaced by a ring of current (Lin et al. 1998, 2002; Titov & Démoulin 1999). As for the above cartesian models, an ideal MHD evolution during the build-up phase also typically, but not always, lead to a loss of equilibrium. The differences will be discussed in Sections 3 and 4. A non equilibrium point could also be present when line-tied conditions are imposed at the photospheric footpoints of the flux rope (Isenberg & Forbes 2007).

From another point of view, Kliem & Török (2006) studied the stability of a toroidal current ring immerged in a background potential field, $\mathbf{B}_p$. Extending the results summarized in Bateman (1978), they derive that an

instability occur when the background field component orthogonal to the torus ($|B_{p,x}|$) decreases faster than $1/h^{3/2}$ with a correction depending on the torus aspect ratio (major over minor radius). Kliem & Török (2006) called it the "torus instability". They analyzed cases where the electric current I was held constant or fixed by the conservation of the total magnetic flux within the torus hole.

The aims of present paper is to revisit the above studies to analyze their relationships. Is this "torus instability" different from the loss of equilibrium found in previous studies with a toroidal current? Has it a different physical origin than the instability of van Tend & Kuperus (1978) obtained with a straight current channel? The Cartesian and axisymmetric models are first written with the same formalism in Section 2. We compare the loss of equilibrium and the instability approaches in both geometries in Section 3, before comparing the criteria of instabilities taking into account a finite current-channel width which evolves during the perturbation (Section 4). Finally, in Section 5, we summarize our results and discuss the relationship between the Cartesian and axisymmetric models, as well as between the loss of equilibrium and the torus instability.

2. BASIC CONCEPTS

The coronal magnetic field $\mathbf{B}$ can always be is written as the sum of a background magnetic field $\mathbf{B}_p$ and the magnetic field $\mathbf{B}_I$, created by localized coronal currents and their images below the photosphere (Section 2.2). $\mathbf{B}_I$ has a vanishing B_z component at $z = 0$ by construction. All the analytical models use this field decomposition with various approximations for $\mathbf{B}_I$. $\mathbf{B}_p$ is most frequently taken as the unique potential field associated with the photospheric "normal magnetogram" $B_z(x, y, 0)$ and with vanishing strength at infinite distance. We consider this case below, however, it is worth noting that, in general, $\mathbf{B}_p$ can also incorporate distributed coronal currents (e.g. $\mathbf{B}_p$ could be a linear force-free field, and $\mathbf{B}_I$ needs to be self consistently computed, Démoulin & Priest 1988).

2.1. Modelization with Concentrated Currents

In order to have a set of equations solvable analytically, simplifications in the magnetic configuration need to be made. A first one is to suppose that the electric current is restricted to a thin channel in the corona (Figure 1 (a)). More precisely that its typical thickness, $2a$, is small compared to the spatial scales of $\mathbf{B}_p$ and to the local radius of curvature of the current channel axis. In an active region, the magnetic shear is typically concentrated around the PIL, while the surrounding arcade is more potential, so electric current are stronger around and above the PIL. With reconnection of sheared loops at the PIL, an important fraction of the currents are inside a twisted flux tube (Aulanier et al. 2010, and references therein). Then, the introduction of a concentrated current channel is motivated by observations and MHD simulations, however it is still an important simplification (e.g., neglecting the effect of more distributed currents as well a the presence of narrow current layers and sheets).

The approximation of a thin current channel allows to separate approximately the magnetic equilibrium in a internal and external equilibrium (Chen 1989; Isenberg et al. 1993). This splitting is better achieved as the current channel is thinner. For the external equilibrium, the Laplace force, integrated over the channel cross section, vanishes, so that there is no average magnetic field component orthogonal to the current channel. The internal equilibrium is solved locally, in the channel cross section. A twisted flux tube has generically both toroidal (axial) and poloidal (azimuthal) magnetic field and electric current components. The equilibrium is typically solved in cylindrical coordinates with a balance between the total magnetic pressure gradient and the tension of the poloidal magnetic field (force-free field solution). This internal equilibrium is not the object of present paper, and we refer to the work of Lin et al. (1998).

Another important simplification is the absence of a neutralization, or return, current around the direct current. Such return current, of opposite direction and with the same magnitude as the direct current, is expected to be present in a magnetic field formed by emergence or induced by localized boundary (photospheric) motions (Parker 1996b). In both cases the complete neutralization is due to a vanishing circulation of $\mathbf{B}$ around a large path enclosing the current channel. Return currents are indeed present in MHD simulations, but when a significant magnetic field component is present along the PIL, the direct current has a larger magnitude than the return current (Török & Kliem 2003; Aulanier et al. 2005). Indeed, only a partial neutralization was typically reported in sunspots (Wheatland 2000; Venkatakrishnan & Tiwari 2009). With partial neutralization, the current intensity, I, is the non-vanishing sum of the two opposite currents.

We argue that the occurence of non fully neutralized currents should be a common feature in solar active regions. The contrary would imply that current-carrying flux tubes should be fully surrounded by potential fields, not only high up in the corona, but also low down around PILs. It is worth noticing, however, that some MHD models for solar eruptions clearly do not require a net current (the magnetic breakout, tether cutting and flux disappearance models, respectively addressed by Antiochos et al. 1999; Moore & Roumeliotis 1992; Amari et al. 2000), as they are based on a gradual diminishing of the tension of the background field, irrespectively of the distribution of electric currents at lower altitudes. Many other models exist (as reviewed e.g. in Forbes et al. 2006; Aulanier et al. 2010), but it is conceivable that several actually fall into the physical frame studied in the present paper.

2.2. Image Current

The lack of significant photospheric magnetic flux evolution during the initiation of a CME can be modeled with the introduction of image currents below the photosphere. The straight channel case of Kuperus & Raadu (1974) can be generalized to any channel shape as illustrated in Figure 1(a). Let the current vector be (I_x, I_y, I_z) at a generic point (x, y, z) of the corona, then the introduction of the image current $(-I_x, -I_y, I_z)$ at the image position $(x, y, -z)$ implies that the vertical component of the magnetic field at the photosphere, $B_z(x, y, 0)$, is unaffected by the presence of the current channel.

The introduction of this image current is a particu-

lar case of the technique of images to impose a particular boundary condition in the setting of electrodynamic problems (Jackson 1975, chap. 2 and 5). Physically, the coronal current path is closing in a complex set of horizontal photospheric currents, which create the same coronal magnetic field than the image current.

2.3. Magnetic flux

We suppose that photospheric evolution and magnetic reconnection are negligible during the instability phase, then the total coronal magnetic flux passing below the current channel is conserved. This flux is the sum of the flux of $\mathbf{B}_\mathrm{p}$ and of $\mathbf{B}_\mathrm{I}$. By the symmetric construction of the image current, the coronal flux of $\mathbf{B}_\mathrm{I}$ is half the flux enclosed by the full current channel (coronal and image current), so it is equal to $LI/2$, where L is the external inductance of the full current channel (e.g. Jackson 1975).

The total inductance of a circular channel of main radius h and of small radius a (Figure 1(b)) is

$$L_\mathrm{c} = \mu_0 h \left(\ln\left(\frac{8h}{a}\right) - 2 + \frac{l_\mathrm{i}}{2} \right), \qquad (1)$$

where μ_0 is the magnetic permeability, and l_i is the normalized internal inductance, per unit length, of the current channel (Grover 1946). l_i take the value of 0, 0.5 or 1 for a current concentrated at the border of the torus, uniformly distributed within the cross section, or with a linear force-free field equilibrium (Lin et al. 1998, and references therein). Equation (1) is simple, but still a good approximation of more complete expressions. For example, it is close to the series expansion tabulated by Malmberg & Rosenbluth (1965) in the range $0.1 < a/h < 1$ for $l_\mathrm{i} = 0$. Moreover, the expression with elliptic integrals given by Ramo et al. (1994, p. 193) is also close to Equation (1) with $l_\mathrm{i} = 0$ in the range $0.15 \leq a/h < 1$, while for lower a/h values it is closer to the case $l_\mathrm{i} = 0.5$. Finally, for the coronal magnetic flux passing below the current channel, the external inductance is required, so the flux is $L_\mathrm{c}I/2$ with $l_\mathrm{i} = 0$.

With the same notations (Figure 1(c)), the total inductance of a straight channel and its image, for a length Δy along the channel, is

$$L_\mathrm{s} = \frac{\mu_0 \Delta y}{\pi} \left(\ln\left(\frac{2h}{a}\right) + \frac{l_\mathrm{i}}{2} \right), \qquad (2)$$

where l_i has the same value than in the above circular case. The main difference with the circular case, is that L_s is only weakly dependent of h so that L_s is almost constant during a global perturbation of the channel (modifying the height h). As above, the coronal magnetic flux passing below the current channel is $L_\mathrm{s}I/2$ with $l_\mathrm{i} = 0$.

2.4. Magnetic Self Force

From the Biot and Savart law, a current channel generates a magnetic field at any point of the space, in particular in the current channel. The component of this field orthogonal to the current channel induces a Laplace force. The direct calculation of this force from the Biot and Savart law is very cumbersome, even for a simple torus geometry. In practice, this force is computed by equaling the work of this force to the change of the magnetic energy ($LI^2/2$) during an elementary displacement, preserving the magnetic flux encircled by the current

channel, LI, so that there is no inductive effect (Shafranov 1966; Garren & Chen 1994). For a circular current channel, this implies an outward radial force f_c, per unit length along the channel, given by:

$$f_\mathrm{c} = \frac{I^2}{2} \frac{\partial L_\mathrm{c}}{\partial h} = I^2 \frac{\mu_0}{4\pi h} \left(\ln\left(\frac{8h}{a}\right) - 1 + \frac{l_\mathrm{i}}{2} \right). \qquad (3)$$

The force f_c is the Laplace force between the toroidal (axial) current and the poloidal magnetic field. There is also the Laplace force between the poloidal current and the toroidal magnetic field inside the twisted flux tube. Taking into account the internal equilibrium, in the limit $a/h << 1$, this second force only gives a small correction to the previous force, as the total force is obtained from Equation (3) by replacing l_i by $l_\mathrm{f} = l_\mathrm{i} - S_h$ with $S_h \approx 1$ (Shafranov 1966). Then, we write the total force as $r_\mathrm{c}I^2$ with

$$r_\mathrm{c} = \frac{\mu_0}{4\pi h} \left(\ln\left(\frac{8h}{a}\right) - 1 + \frac{l_\mathrm{f}}{2} \right) \qquad (4)$$

The local outward force $r_\mathrm{c}I^2$, called hoop force, has its origin in the magnetic field created by each of the elementary part of the circular ring, with the largest contribution coming from the closest currents. Indeed, it has a logarithm divergence as the small radius, a, becomes smaller. For $a << h$ the logarithm term slightly dominates in Equation (4). If the current channel is fully in the corona (e.g. Lin et al. 1998), Equation (4) includes only the self-force of the coronal current channel, whereas if the current channel is only half in the corona (e.g. Lin et al. 2002, Figure 1(b)) Equation (4) also includes the force from the image current. Finally, Garren & Chen (1994) have generalized these results to current channels with arbitrary shapes.

For a straight current channel, located at the height h above the photosphere, the magnetic force can be computed as above (Equation (3)) with L_c replaced by L_s or the magnetic field of the image current can be computed first by the Biot and Savart law. The repulsion function r_s is

$$r_\mathrm{s} = \frac{\mu_0}{4\pi h}. \qquad (5)$$

r_s has indeed a similar form as r_c (Equation (4)) since the logarithm term provides only a weak dependance on h/a.

3. LOSS OF EQUILIBRIUM AND INSTABILITY

3.1. Magnetic Field Evolution

The MHD evolution of the coronal magnetic field of an active region, outside flare times, has typically three time-scales, as follows. The shortest time-scale, τ_A, called the Alfvén time, is given by the typical time that Alfvén waves require to cross the coronal field configuration. Outside of the eruption period, the magnetic configuration is not significantly changing on such time scale and Alfvén waves transport the magnetic stresses (shear, twist). On an intermediate time-scale, τ_B, the coronal magnetic stress is significantly changing, for example because of sub-photospheric torsional Alfvén waves are bringing twist to the coronal field, or because of reconnection between sheared magnetic loops is forced by converging flows at the PIL. On this intermediate time-scale, coronal currents significantly change, but not the global

photospheric distribution of the magnetic field component normal to the photosphere (i.e. the "normal magnetogram"). On the longest time-scale, τ_C, both the coronal currents and the "normal magnetogram" are evolving.

For a mature AR, with a magnetic flux of $\approx 10^{22}$ Mx, the above time-scales are typically of the order of $\tau_A \approx$ few minutes, $\tau_B \approx$ few days, and a $\tau_C \approx$ week to months. They are well separated, a useful property for an analytical study since it allows to isolate the main physics involved for each time-scale. Thus, we can use different approximations to analyze the magnetic field evolution on these time-scales, as follows. The global stability of the equilibrium can be tested with ideal MHD on the shortest time-scale τ_A. On the intermediate time-scale τ_B, the build up of coronal current can be studied within a given potential $\mathbf{B}_p$ (computed uniquely from the "normal magnetogram", using appropriate boundary conditions on the sides of the domain). Finally the evolution on the longest time-scale τ_C is mostly studied with MHD simulations or with analytical studies imposing an ideal-MHD evolution.

3.2. Loss of Equilibrium with a Circular Current Channel

First, we revisit the model proposed by Titov & Démoulin (1999), keeping it the simplest as possible. The potential field $\mathbf{B}_p$ is created by two magnetic sources, of equal flux ϕ but of opposite sign, located at $x = \pm D, y = z = 0$ and by a line current located at $y = z = 0$. The magnetic field of this line current adds a contribution to the coronal potential field, but it does not modify the equilibrium, nor the equilibrium perturbation studied below, so this field is not present in the following equations (the aim of this magnetic field is only to have a finite twist in the coronal field). A torus of electric current, centered at $x = y = z = 0$, is introduced in the plane y-z (Figure 1(b)). Since the photospheric boundary is set at $z = 0$, the half part of the torus at $z < 0$ represents the image current.

The magnetic configuration considered is axisymmetric (around the x-axis), then the magnetic force on the current channel is radial in the y-z plane with the same value along the current channel:

$$f = r_c I^2 + B_{p,x} I, \tag{6}$$

where r_c is given by Equation (4). The x-component of $\mathbf{B}_p$ at the current location is:

$$B_{p,x} = -4\phi D(h^2 + D^2)^{-3/2}. \tag{7}$$

The equilibrium current, $I_{eq.}$ is given by $f = 0$ in Equation (6):

$$I_{eq.}(h) = \frac{16\pi}{\mu_0} \frac{\phi D h (h^2 + D^2)^{-3/2}}{\ln(8h/a) - 1 + l_f/2}. \tag{8}$$

Starting from a nearly potential configuration (small I value), if the current value could be progressively increased in function of time as in a classical electric circuit, then a loss of equilibrium would occur when I would reach the maximum value of $I_{eq.}(h)$. The circular current channel behaves in the same way as a straight current channel and its image current (Figure 1(c) and Section 3.6) as proposed by van Tend & Kuperus (1978).

However, with an MHD evolution, the magnitude of the coronal current is rather determined by the magnetic field evolution, so its time evolution cannot be imposed a priori. Indeed, during a typical MHD evolution with imposed photospheric velocities, the coronal current magnitude first grows then later decreases (e.g. Aly 1985; Klimchuk & Sturrock 1989; Aulanier et al. 2005).

In previous studies, the magnetic field evolution is typically assumed to be ideal (e.g. Isenberg & Forbes 2007, and references therein). With no magnetic flux emerging or canceling between the photospheric sources (located at $x = \pm D$), this implies the conservation of the magnetic flux, F, through the area, S, defined between $z = 0$ and the bottom of the current channel. F is given by

$$F = \frac{L_e I}{2} + \iint_S B_{p,x} \, dy \, dz \tag{9}$$

$$= \frac{L_e I}{2} - 4\pi\phi \left(1 - \frac{D}{\sqrt{(h-a)^2 + D^2}}\right), \tag{10}$$

with $L_e = \mu_0 h(\ln 8h/a - 2)$ is the external inductance of the current channel (see Equation (1)). The conservation of F, together with the time evolution of one parameter of the model (e.g. ϕ or D) provides an evolution constraint with the generic form $I_{evol.}(h)$. Its intersection with the equilibrium curve, $I_{eq.}(h)$, determines the evolution of I in function of the evolving parameter (e.g. ϕ or D).

With a circular current channel, Lin et al. (2002) has shown that evolving D, with F preserved, does not lead to a loss of equilibrium, but rather to a self similar evolution of the configuration (which is just a rescale in size). However, they also show that a decrease of ϕ does lead to a loss of equilibrium. Figure 2(a) is a graphical representation of this result. As in previous studies, the maximum of $I_{eq.}(h)$ defines the reference state with fluxes ϕ_0 and F_0. The evolution is parametrized by f_ϕ defined by $\phi = f_\phi \phi_0$, where f_ϕ is a decreasing function of time as observed after the emerging phase of an active region (e.g. van Driel-Gesztelyi et al. 2003) or before filament eruption (e.g. Schmieder et al. 2008). In order to have an equilibrium curve not evolving with ϕ (to simplify the graphic), we draw $I_{eq.}/\phi$ (normalized to its maximum value), as well as $I_{evol.}/\phi$.

Starting the evolution with $f_\phi > 1$, the constraint $F = F_0$ has an intersection with the equilibrium curve before its maximum (e.g. at the point "a" for $f_\phi = 1.5$ in Figure 2(a)). This equilibrium is stable since the perturbed equilibrium, with the constraint $F = F_0$, has a restoring force as shown with the arrows (see Section 4.1 for the analysis of the perturbed equilibrium).

As f_ϕ decreases (due e.g. to magnetic flux cancelation with some photospheric flux brought from $|x| > D$), the equilibrium height h increases. Contrary to what is obtained if the evolution of I is prescribed as in a circuit model, the conservation of magnetic flux in ideal MHD leads to the equilibrium to be still stable after the maximum of $I_{eq.}/\phi$ (point "b"), up to the point "c".

For larger h values, e.g. at point "a′", the equilibrium is unstable to an ideal perturbation (i.e with F preserved). However, this unstable region is not reachable during the pre-eruptive evolution: the quasi-static evolution ends at point "c" with both an equilibrium becoming unstable (see arrows in Figure 2(a)) and without
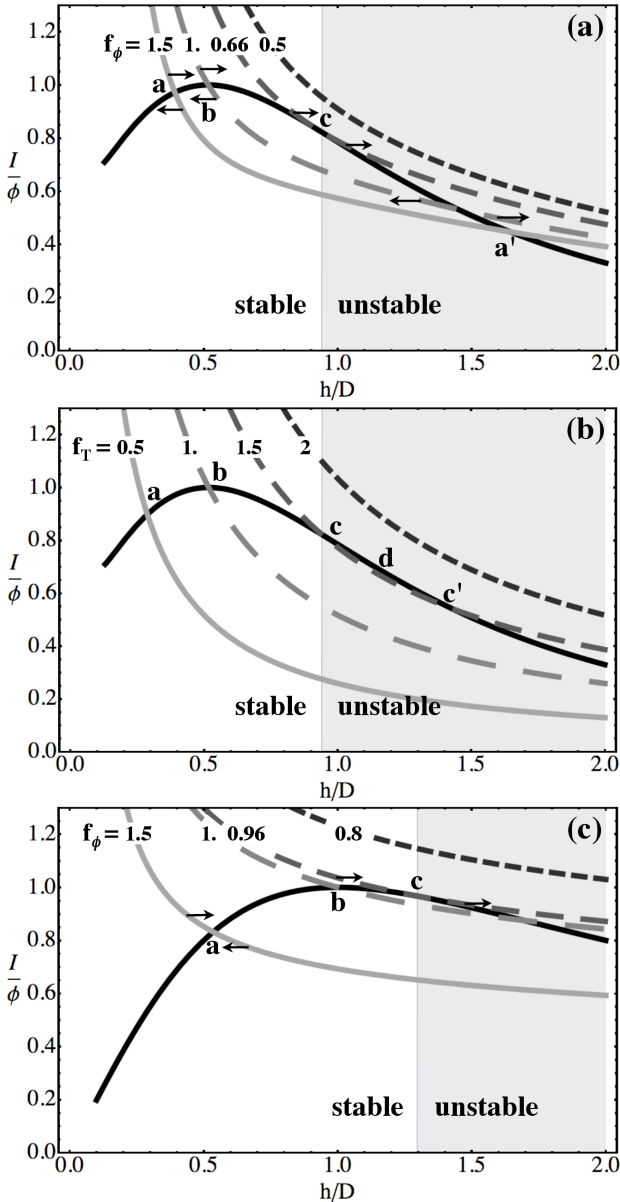
FIG. 2.— The coronal electric current, I, divided by the photospheric magnetic flux ϕ, in function of the coronal height h, normalized to half the x distance, D, of the photospheric magnetic polarities. The equilibrium curve, $I_{eq.}/\phi(h)$, is in black, while the evolution constraint is shown in grey/dashed style for four values of the evolution factor f. Both f and $I_{eq.}/\phi$ are normalized to 1 at the maximum of $I_{eq.}/\phi$. **(a,b)** Case of a circular current channel (Figure 1(b)), **(c)** case of a straight current channel (Figure 1(c)). **(a,c)** The photospheric flux, ϕ, is evolved with the factor $f = f_\phi$. **(b)** The magnetic twist of the flux tube is evolved with the factor $f = f_T$. Arrows represent the direction of the force when the system is perturbed away from the equilibrium.

neighbor equilibrium, as f_ϕ is slightly more increased, so there is a loss of equilibrium. The evolution sequence with decreasing f_ϕ ends with a fast evolution driven by an outward force, so an eruption. It could be confined if a stable equilibrium would be present at greater height, e.g. due to the formation of a long current sheet below the flux rope (Forbes & Isenberg 1991), or if a too strong magnetic tension of the overlying field would be present (as for the kink-unstable eruption modeled by Török & Kliem 2005).

3.3. Other Possible Evolutions on Intermediate Time Scales

The analysis of the previous section supposes an ideal-MHD evolution to progressively shift the equilibrium to a point of the equilibrium curve where no neighbor equilibrium exists (with the magnetic flux conservation). This is only one plausible scenario for solar eruptions (see Section 1). Indeed, on the intermediate time-scale τ_B, magnetic reconnection can play a crucial role in transforming the coronal field. For example, this is the case with a progressive diffusion of photospheric magnetic polarities leading to reconnection at the PIL and the transformation of sheared to twisted field lines, contributing to build up the twisted flux tube and the associated current channel (as in the numerical simulations of Amari et al. 2003; Fan & Gibson 2004; Mackay & van Ballegooijen 2006; Aulanier et al. 2010). A progressive transformation of the coronal magnetic configuration is also expected due to reconnection of the current layers formed at separatrices and Quasi-Separatrix Layers (QSLs, e.g. Titov et al. 2002) during the intermediate time-scale τ_B. We conclude that typically it is not obvious to justify an ideal-MHD evolution during the long pre-eruptive build-phase before an eruption, on time scales much longer than τ_A, and in particular using the evolution constraint of a preserved flux below the flux rope (e.g. Equation (10)).

More generally, for a given observed configuration or in a 3D MHD simulation, it is difficult to determine the main evolutionary constraint, even with detailed analysis (e.g. Aulanier et al. 2010). This is not due to a lack of available data; rather, the difficulty is due to the complexities inherent in the 3D evolution of magnetic fields. This is illustrated by the formidable complexity of studying the loss of equilibrium even in a simplified configuration (e.g. a small bipole emerging in a bipolar field, Lin et al. 2001).

3.4. Instability with a Circular Current Channel

Let us illustrate another possible evolution than the ideal-MHD evolution on the time scale τ_B. This following case is selected mainly because of its simplicity to illustrate other possible evolutions. The current channel is associated with a twisted flux tube which has a finite twist due to the presence an axial magnetic field. The average coronal twist, T, is approximately related to the current I and the toroidal flux, ϕ_t, in the flux rope by (see Equation(9) in Titov & Démoulin 1999):

$$T = \mu_0 I h \, / \, (2\phi_t). \qquad (11)$$

Let us suppose that the flux rope twist T is increasing, e.g. due to torsional Alfvén waves coming from the convective zone, or as a consequence of reconnecting sheared loops (increasing the flux rope flux). Equation (11) provides a new evolution constraint, replacing the conservation of F used in Section 3.2. As previously, the maximum of $I_{eq.}(h)$ defines the reference state with the flux ϕ_0 and the twist T_0. Here, we simply suppose that the photospheric field sources are not evolving so $\phi = \phi_0$, but we still plot $I_{eq.}/\phi$ for coherence with previous case. The evolution is parametrized by f_T defined by $T = f_T T_0$.

Starting the evolution with $f_T < 1$, the evolution constraint, Equation (11), has an intersection with the equilibrium curve before its maximum (e.g. at the point "a"

for $f_T = 0.5$ in Figure 2(b)). As in Section 3.2, this equilibrium is stable. As f_T increases, the equilibrium height h increases, reaching point "b" then point "c". If we only consider the evolution constraint, the evolution would reach point "d", where no neighbor equilibrium is present when f_T is further increased. As in the previous case (in Figure 2(a)) a loss of equilibrium is present, but at larger height.

However, the true physical evolution of the system is ending earlier, at point "c", where the system is unstable on the short time scale τ_A with an ideal-MHD perturbation (preservation of the flux F in Equation (10), while the evolution of T is negligible on the short time scale τ_A).

3.5. *Loss of Equilibrium or Instability?*

In the two previous evolutions (Figures 2(a) and (b)) the eruption occurs at the same location along the equilibrium curve, at the point "c". However, they appear to have a different theoretical origin. In the first case (Figure 2(a)) the progressive decrease of f_ϕ brings the system to point "c" where no neighbor equilibrium exits with a further decrease of f_ϕ. In the second case (Figure 2(b)) the increase of f_T brings also the system to point "c", but a neighbor equilibrium is present with a further increase of f_T (up to point "d"). Simply, the equilibrium after point "c" is unstable with an ideal perturbation (F preserved), and as in the first case, an upward eruption is present after the system reaches point "c". Indeed, on the time scale τ_A, the evolution of the two cases will be the same after they reach point "c", since the same unstable force (Equation (6)) is acting with the constraint of an ideal-MHD evolution (so preserving F in Equation (10)). Then, we argue that there is no point to discuss whether there is a loss of equilibrium or a transition from a stable to an unstable equilibrium.

More generally, for an observed coronal field evolution, and even for an MHD simulation (where all physical quantities are available in the volume), we claim that, in most cases, it will be at least difficult, if not impossible, to define precisely the evolution constraint as in the previous two cases. Indeed, with a slow enough driving, the system follows the equilibrium curve, and the extensions away from this curve, along the evolution constraint, are purely theoretical considerations which are available only if an analytical analysis is achievable. In a magnetic configuration which includes some separatrices or QSLs, so with some reconnection, we claim that an evolution constraint cannot generically be constructed. However, a generic approach is to test the ideal-MHD stability all along the evolution (within the limit of numerical dissipation for MHD simulations).

Because of the separation of the time scale of the coronal evolution (τ_A) from the longer times scales of the photospheric evolution (τ_B, τ_C, see Section 3.1), the magnetic configuration cannot reach the equilibrium branch at an altitude h larger than that of the point "c" by a slow quasistatic evolution, which does correspond to observed pre-eruptive evolutions. Reaching a region of the equilibrium curve beyond "c" may be dynamically possible, but only for fast (e.g. Alfvénic) evolutions of magnetic configurations being out of equilibrium. This is, however, not observed in the Sun's atmosphere, even during flux emergence. Nevertheless, considering an an-

alytical model of the equilibrium, one can always start a numerical simulation from any point along the equilibrium curve, stable or unstable (e.g. Török & Kliem 2007). The unstable branch is unaccessible for a coronal field, except the vicinity of point "c" which can be reached with a small but finite velocity due to the slow evolution present in the pre-eruptive stage. Indeed, including such small velocity implies an evolution curve, $h(t)$, which is in better agreement to observed $h(t)$ in prominence eruptions, than letting the instability grows from an initial very small perturbation (Schrijver et al. 2008).

3.6. *Loss of Equilibrium with a Straight Current Channel*

The evolution summarized Figures 2(a) and (b) is expected to be generic of magnetic configurations having at least one current channel which is not fully neutralized since the hoop force is generically present with a curved current channel (Garren & Chen 1994). Indeed, this has been shown in more complex configurations, even by including a complete photospheric line tying, i.e. not only fixing the "normal magnetogram" (with the inclusion of image current, see Section 2.2), but also fixing the photospheric positions of the current channel (Isenberg & Forbes 2007).

However, the above physical evolution is not limited to the presence of the hoop force. It is indeed generic of the Lorentz force created by any current channel. At a given position of the circuit, the magnetic force can be dominated either by the magnetic field created by the current located in the vicinity of this position (hoop force) or by the current at large distance (e.g. an image current). Indeed, van Tend & Kuperus (1978) first proposed a catastrophe model of a straight current channel embedded in a potential field.

As in Section 3.2, a potential field $\mathbf{B}_p$ is introduced to achieve an equilibrium. As previously, we select a bipolar field $\mathbf{B}_p$ created by two magnetic sources of flux ϕ located at $x = \pm D, z = 0$, but now invariant by translation in the y direction. The x-component of $\mathbf{B}_p$ at the current location is:

$$B_{p,x} = -2\phi D(\pi(h^2 + D^2))^{-1} . \quad (12)$$

The equilibrium current, $I_{eq.}$ is given by $f = 0$ in Equation (6):

$$I_{eq.}(h) = \frac{8\pi}{\mu_0} \frac{\phi D h}{h^2 + D^2} . \quad (13)$$

The equilibrium curve is closely similar to the one found for a circular current channel (compare panels a and c of Figure 2). The main difference is that the maximum of $I_{eq.}$ is shifted to a larger height. This is mainly due to the different dependance with h of $B_{p,x}$ for a 2D and 3D bipole. Much closer equilibrium curves are obtained when the 2D bipole is replaced by a 2D quadrupole (giving a potential-field dependance similar to Equation (7)).

The conservation of the magnetic flux below the current channel, per unit length along its axis (Equation (9)), for the straight channel case is:

$$F = \frac{\mu_0 I}{2\pi} \ln \frac{2h}{a} - \frac{2\phi}{\pi} \tan^{-1} \frac{h - a}{D} . \quad (14)$$

A major difference with the circular case is that the constraint of F conservation implies that I has a much

weaker dependence on h (Figure 2(c)). It implies that the ideal-MHD instability occurs just after the maximum of $I_{\text{eq.}}/\phi$ (where $f_\phi = 1$), when the photospheric polarities have weaken by only 4% ($f_\phi = 0.96$). Indeed, the ideal-MHD evolution leads to a non equilibrium at a location nearby to the one found by van Tend & Kuperus (1978) with an evolution simply driven by an increase of the current I.

As for the circular current channel, a loss of equilibrium at point "c" is only present if the magnetic evolution is fully ideal. More generally, whatever is the driver of the evolution on the time scale τ_B, the system is becoming unstable as it reaches point "c", and it is ideally driven away from the equilibrium curve by the same force in the short time scale τ_A.

3.7. *Comparison to Previous Studies*

Based on our analysis above, we can now answer to the following question: is there a major difference in the following approaches: "loss of equilibrium" studies with straight or circular current channel (e.g. van Tend & Kuperus 1978; Lin et al. 2002), and the "torus instability" (Kliem & Török 2006) previously studied in the tokamak laboratory experiment (e.g. Bateman 1978)?

First, the straight or circular current channels have very similar repulsion forces, $r(h)I^2$, implying the same kind of equilibrium curve. Indeed, for a circular current channel, $r_c(h)$ has a contribution from both the coronal part ($z > 0$) and from the image current ($z < 0$). Simply, both contributions can be combined in a single term, Equation (4), masking the contribution of the image current. More generally, Garren & Chen (1994) have derived a general expression for $r(h)$ for arbitrary current shapes. r_c and r_s (Equations (4) and (5)), are simply two limits of the same $r(h)$, for circular and straight current channels.

Next, Kliem & Török (2006) studied the "torus instability" of a circular current channel imposing a constant current I or a constant flux F. The first case is directly comparable to the work of van Tend & Kuperus (1978) and the second case to the work of Lin et al. (2002). The only significant difference is that Kliem & Török (2006) study the stability of the equilibrium curve (Figure 2(a)), but do not follow the evolution of the magnetic configuration on intermediate time scale τ_B (so they cannot detect the presence or not of a loss of equilibrium).

The main difference between the loss of equilibrium and the stability analysis is that, for the first case, a precise way how the system can evolve to instability is proposed, while, in the second case, one only tests the stability of a given equilibrium (which could be physically inaccessible). However, with both type of analyses, an ideal instability is present at the same location of the equilibrium curve if the same equilibrium is analyzed. This last condition is not trivial if one allows the formation of current sheets during the long-term evolution (on the time scale τ_B).

4. EQUILIBRIUM STABILITY

We study below the stability of the magnetic configuration around an equilibrium position. The main assumption is that the magnetic force balance is the same at any position along the current channel, so that the magnetic force can written as in Equation (6). This in-

cludes both circular and straight current channels in the same formalism. The stability of the configuration is first derived in this general framework in Section 4.1, with the constraint of magnetic flux conservation derived in Section 4.2. These results are used for the particular cases studied in previous section. Finally a parametric study of the stability is presented.

4.1. *Force Perturbation*

The magnetic force, $f(a, h, I)$, on the current channel is described by Equation (6). A perturbation $(\mathrm{d}a, \mathrm{d}h, \mathrm{d}I)$ around the equilibrium, $f(a, h, I) = 0$, creates the force $\mathrm{d}f$ as

$$\mathrm{d}f = \frac{\partial f}{\partial a}\mathrm{d}a + \frac{\partial f}{\partial h}\mathrm{d}h + \frac{\partial f}{\partial I}\mathrm{d}I\,. \qquad (15)$$

During a perturbation the radius a is evolving as given by the internal force balance. With a linear force-free field inside the flux rope and ideal MHD, Lin et al. (1998) found that a evolves as $1/I$. Here we include a more general variation, supposing $a(I)$, and we introduce the index of variation of a with I

$$n_{\text{a}} \equiv -\frac{\partial \ln a}{\partial \ln |I|}\,, \qquad (16)$$

so $n_{\text{a}} = 1$ for the internal evolution included in Lin et al. (1998). Then, Equation (15) is rewritten as

$$\mathrm{d}f = \left(\frac{\partial f}{\partial h} + \left(-n_{\text{a}}\frac{a}{I}\frac{\partial f}{\partial a} + \frac{\partial f}{\partial I}\right)\frac{\mathrm{d}I}{\mathrm{d}h}\bigg|_{\text{pert.}}\right)\mathrm{d}h\,, \quad (17)$$

where $\mathrm{d}I/\mathrm{d}h|_{\text{pert.}}$ express how the current intensity is modified during the perturbation.

If the perturbation is realized along the equilibrium curve, the force $\mathrm{d}f$ has the same expression except that $\mathrm{d}I/\mathrm{d}h|_{\text{eq.}}$, computed along the equilibrium curve, replaces $\mathrm{d}I/\mathrm{d}h|_{\text{pert.}}$ in Equation (17). Also in this case, $\mathrm{d}f = 0$ so

$$\frac{\partial f}{\partial h} + \left(-n_{\text{a}}\frac{a}{I}\frac{\partial f}{\partial a} + \frac{\partial f}{\partial I}\right)\frac{\mathrm{d}I}{\mathrm{d}h}\bigg|_{\text{eq.}} = 0\,, \qquad (18)$$

where we suppose that the internal equilibrium has the same n_{a} index. Using the equilibrium condition, $f = r\,I^2 + B_{\text{p,x}}I = 0$, and Equation (18), Equation (17) is rewritten as

$$\mathrm{d}f = r\,I\left(1 - n_{\text{a}}\frac{\partial \ln r}{\partial \ln a}\right)\left(\frac{\mathrm{d}I}{\mathrm{d}h}\bigg|_{\text{pert.}} - \frac{\mathrm{d}I}{\mathrm{d}h}\bigg|_{\text{eq.}}\right)\mathrm{d}h\,. \quad (19)$$

The equilibrium is unstable when $\mathrm{d}f$ and $\mathrm{d}h$ have the same sign. Then, an instability is present when the absolute value of the current in the perturbation decreases less rapidly with height than along the equilibrium curve. This is illustrated in Figure 2.

On the short time-scale τ_A, the perturbation is described by ideal MHD, with a preservation of the flux distribution at the boundary $z = 0$ (so ϕ =constant in the examples of Section 3.2 and 3.6). Then, a perturbation corresponds to a small excursion away from the equilibrium curve with the constraint of magnetic flux conservation in Figures 2(a) and (c). The tangent point "c" between the equilibrium curve and the constraint of flux conservation define both the limit of the stable region and the non equilibrium point (in an ideal evolution on the time-scale τ_B).

Using the equilibrium condition to specify $\mathrm{d}I/\mathrm{d}h|_{\mathrm{eq.}}$, the force perturbation, Equation (17), is rewritten as

$$\frac{\mathrm{d}f}{\mathrm{d}h} = r\,I\left(1 - n_{\mathrm{a}}\frac{\partial \ln r}{\partial \ln a}\right)\frac{\mathrm{d}I}{\mathrm{d}h}\bigg|_{\mathrm{pert.}} + I\frac{\partial B_{\mathrm{p,x}}}{\partial h} + I^2\frac{\partial r}{\partial h}\,. \tag{20}$$

We define the decay index of the potential field as

$$n_{\mathrm{Bp}} \equiv -\frac{\partial \ln |B_{\mathrm{p,x}}|}{\partial \ln h}\,. \tag{21}$$

This decay index is introduced in Equation (20) by dividing $\mathrm{d}f$ by $B_{\mathrm{p,x}}I$, or equivalently by $-r\,I^2$, and by multiplying by h. Finally, the equilibrium is unstable (i.e. $\mathrm{d}f/\mathrm{d}h > 0$) if

$$n_{\mathrm{Bp}} > n_{\mathrm{Bp,crit.}} \equiv n_{\mathrm{r}} + n_{\mathrm{I}}$$
$$\equiv -\frac{\partial \ln r}{\partial \ln h} - \left(1 - n_{\mathrm{a}}\frac{\partial \ln r}{\partial \ln a}\right)\frac{\mathrm{d}\ln|I|}{\mathrm{d}\ln h}\bigg|_{\mathrm{pert.}} \tag{22}$$

so if the potential field decreases fast enough with height. The instability threshold depends on how fast the repulsion decreases with height (given by the decay index n_{r}) and on how much the current is allowed to decrease during the perturbation (given by the decay index n_{I}).

4.2. Constraint of Flux Conservation

The decay index n_{I} is computed from an ideal MHD constraint, as follows. On the short time-scale τ_A, the perturbation is described by ideal MHD, with the preservation of the coronal magnetic flux F present below the flux rope. With a small perturbation $\mathrm{d}h$, Equation (9) implies

$$\mathrm{d}F = \left(\frac{\mathrm{d}L_{\mathrm{e}}}{\mathrm{d}h}I + L_{\mathrm{e}}\frac{\mathrm{d}I}{\mathrm{d}h}\bigg|_{\mathrm{pert.}} + P\,B_{\mathrm{p,x}}\right)\frac{\mathrm{d}h}{2} = 0\,, \tag{23}$$

where P is the perimeter (or length) of the full current channel, including its image.

The external inductance L_{e} (computed with $l_{\mathrm{i}} = 0$) depends generically on the spatial extension of the current channel (described here only by h) and on the thickness of the current channel (its radius a). Then, the variation of the external inductance with height is

$$\frac{\mathrm{d}L_{\mathrm{e}}}{\mathrm{d}h} = \frac{\partial L_{\mathrm{e}}}{\partial h} + \frac{\partial L_{\mathrm{e}}}{\partial a}\frac{\partial a}{\partial I}\frac{\mathrm{d}I}{\mathrm{d}h}\bigg|_{\mathrm{pert.}}$$
$$= \frac{\partial L_{\mathrm{e}}}{\partial h} - n_{\mathrm{a}}L_{\mathrm{e}}\frac{\partial \ln L_{\mathrm{e}}}{\partial \ln a}\frac{\mathrm{d}\ln|I|}{\mathrm{d}h}\bigg|_{\mathrm{pert.}}\,. \tag{24}$$

The conservation of the magnetic flux, Equation (23), together with Equation (24) imply the following decay index

$$n_{\mathrm{I}} = \frac{1 - n_{\mathrm{a}}\frac{\partial \ln r}{\partial \ln a}}{1 - n_{\mathrm{a}}\frac{\partial \ln L_{\mathrm{e}}}{\partial \ln a}}\left(\frac{\partial \ln L_{\mathrm{e}}}{\partial \ln h} - \frac{P\,h\,r}{L_{\mathrm{e}}}\right)\,. \tag{25}$$

The last factor in the previous equation is due to the conservation of the magnetic flux from the current I minus the flux from the potential field passing below the current channel. The fraction includes the effect of the channel expansion on the repulsion function at the numerator and on the conservation of flux at the denominator. They are both larger than 1 for $n_{\mathrm{a}} > 0$, and they are a growing function of n_{a}. Then, the dependance of r and L_{e} on a have opposite effects on the stability.

4.3. Example of a Circular Current Channel

We apply in this subsection the above results to a circular current channel (Figure 1(b)). The external inductance L_{e} is given by Equation (1), without the contribution of the internal inductance ($l_{\mathrm{i}} = 0$). The repulsion r is given by Equation (4) and $P = 2\pi h$. The contribution from the potential field to the decay index n_{I} is (for $n_{\mathrm{a}} = 0$, i.e. for a constant during the evolution):

$$-\frac{P\,h\,r}{L_{\mathrm{e}}} = -\frac{1}{2}\left(1 + \frac{1 + l_{\mathrm{f}}/2}{\ln(8h/a) - 2}\right)\,. \tag{26}$$

The contribution from the field created by the current channel to the decay index n_{I} is (for $n_{\mathrm{a}} = 0$)

$$\frac{\partial \ln L_{\mathrm{e}}}{\partial \ln h} = 1 + \frac{1}{\ln(8h/a) - 2}\,, \tag{27}$$

so exactly twice the negative contribution from the potential field for $l_{\mathrm{f}} = 0$. For $a \ll h$, i.e. a very thin current channel, the denominator, $\ln(8h/a) - 2$, is relatively large so that the above contributions are close to $-1/2$ and $+1$, respectively. Including Equations (26,27) in Equation (25), and using Equation (1), the decay index n_{I} for the circular current channel is

$$n_{\mathrm{I}} = \frac{(u + l_{\mathrm{f}}/2 + n_{\mathrm{a}})(u - l_{\mathrm{f}}/2)}{2(u - 1 + n_{\mathrm{a}})(u + l_{\mathrm{f}}/2)}\,, \tag{28}$$

with the notation

$$u = \ln(8h/a) - 1\,. \tag{29}$$

Using Equation (4), the decay index of the repulsion r is:

$$n_r = -\frac{\partial \ln r}{\partial \ln h} = 1 - \frac{1}{u + l_{\mathrm{f}}/2}\,. \tag{30}$$

From Equation (22), n_r is the critical decay index of $\mathbf{B}_{\mathrm{p}}$ for instability if the current I would be preserved during the perturbation. n_r is always lower than 1, especially for flux rope with large radius a.

Combining the results of Equations (28,30), the instability condition for a circular current channel is

$$n_{\mathrm{Bp}} > \frac{3}{2} - \frac{(1 + l_{\mathrm{f}}/2)(u - 2 + 2n_{\mathrm{a}} + l_{\mathrm{f}}/2)}{2(u + l_{\mathrm{f}}/2)(u - 1 + n_{\mathrm{a}})}\,. \tag{31}$$

In the limit of a very thin current channel ($a \ll h$), the instability threshold is close to $3/2$, as found in tokamak studies (e.g. Bateman 1978). This corresponds to the "torus instability" for solar eruptions (Kliem & Török 2006), but with a different correction term to $3/2$, as we have not supposed a self similar expansion of the current channel, but rather a dependance $a(I)$.

4.4. Example of a Straight Current Channel

We follow the same derivation than in previous subsection but for a current channel formed by two parallel lines (Figure 1(c)). In this geometry, the external inductance L_{e} is given by Equation (2), again with $l_{\mathrm{i}} = 0$. The repulsion r is given by Equation (5) and $P = 2\Delta y$ (with $\Delta y \gg h, D$). For $n_{\mathrm{a}} = 0$, the contribution from the field created by the current channel to the decay index n_{I}, Equation (25), is exactly twice the contribution from the potential field, but with opposite sign (as above for the circular channel, with $l_{\mathrm{f}} = 0$)

$$\frac{\partial \ln L_{\mathrm{e}}}{\partial \ln h} = 2\frac{P\,h\,r}{L_{\mathrm{e}}} = \frac{1}{\ln(2h/a)}\,. \tag{32}$$
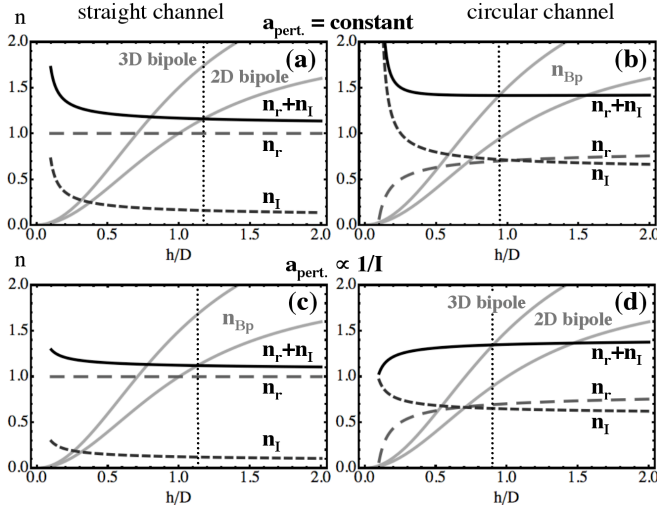
FIG. 3.— Dependence of the decay indexes $n_r = -\partial \ln r / \partial \ln h$, $n_I = -\partial \ln |I| / \partial \ln h$ and $n_{Bp} = -\partial \ln |B_{p,x}| / \partial \ln h$ for a straight (resp. circular) current channel in the left (resp. right) column. The critical index $n_{Bp,crit.} = n_r + n_I$ for instability is shown with a black continuous line. The decay indexes of 2D and 3D potential bipoles are shown in both columns for reference. The dotted vertical line indicates the critical height (point "c" in Figure 2). All panels are drawn with the normalized equilibrium radius $a/D = 0.1$ and for $h > a$. The top (resp. bottom) panels have $n_a = -\partial \ln a / \partial \ln |I| = 0$ (resp. $n_a = 1$).
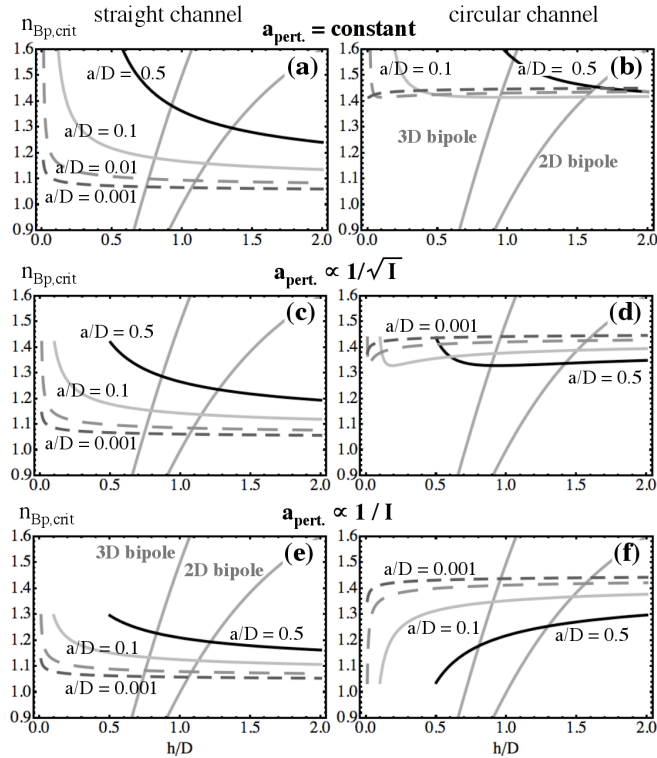
FIG. 4.— The critical index $n_{Bp,crit.} = n_r + n_I$ for instability with various equilibrium radius a normalized by D (half distance between photospheric field concentrations). The results are for a straight (resp. circular) current channel in the left (resp. right) column. The flux rope expands more during the perturbation (larger n_a value) from top ($n_a = 0$) to bottom ($n_a = 1$). The $n_{Bp,crit.}$ curves are drawn for $h > a$. The decay indexes, n_{Bp} of 2D and 3D potential bipoles are shown in both columns for reference.

With Equation (5), the decay index of the repulsion r is simply $n_r = 1$. Combining the above results, the instability condition, Equation (22), for a straight current channel is

$$n_{Bp} > 1 + \frac{1}{2(\ln(2h/a) + n_a)} . \qquad (33)$$

In the limit of a very thin current channel ($a \ll h$), the instability threshold is close to 1, as found by van Tend & Kuperus (1978).

4.5. Comparaison of Circular and Straight Current Channels

From Equation (22), the critical decay index of the potential field for instability, $n_{Bp,crit.}$ has two contributions: the decay indices of the repulsion, n_r, and the decay index of the current during the ideal perturbation, n_I. The main difference of stability between the above two current channels is a much lower index n_I for a straight channel (Figure 3). This is due to the low dependance of L_e on the height h (compare Equation (2) to Equation (1)). In the limit $a \ll h$, this is the origin of a more stable circular current channel ($n_{Bp,crit.} \approx 3/2$) than a straight current channel ($n_{Bp,crit.} \approx 1$). However, this limit is not applicable to the eruptive coronal configurations since it requires extremely thin current channels: for example, even with $a/D = 10^{-3}$, this limit is only weakly approached (Figure 4). This is due to the $\ln(h/a)$ dependance in both Equations (31) and (33).

Moreover, the above difference is partly compensated by a lower decay index of the repulsion, n_r, for a circular channel (as the repulsion, $r(h)$, is decreasing slower with height, especially for large values of a). The net result is that the critical decay index, $n_{Bp,crit.}$, for circular and straight channels, with finite radius a, are much closer than in the limit $a \ll h$. This is illustrated in Figure 3 with $a/D = 0.1$, which still corresponds to a relatively narrow channel. This effect is amplified with a flux rope having a larger expansion during the perturbation, so a larger n_a value, because the contribution of n_I to $n_{Bp,crit.}$ is reduced. Indeed, even with a relatively thin flux rope, $a/D = 0.1$, and an internal expansion rate $n_a = 1$, as in Lin et al. (1998), $n_{Bp,crit.}$ values are close for circular and straight current channels: ≈ 1.3 and ≈ 1.1, respectively (Figure 3(c) and (d)). They correspond to a comparable critical height ($h/D \approx 1$) for straight and circular channels with a 2D and 3D bipole (Equations (7) and (12), respectively).

In previous studies, the instability threshold $n_{Bp,crit.}$ was typically taken in the limit of very thin current channels (e.g. van Tend & Kuperus 1978; Kliem & Török 2006). The above analytical theory is indeed done in the limit of thin current channels (typically $a/D \leq 0.1$). In fact, relatively broad current channels are expected in the coronal with magnetic extrapolations (e.g. Schrijver et al. 2008; Savcheva & van Ballegooijen 2009) and are present in MHD simulations (e.g. Fan & Gibson 2004; Török & Kliem 2007; Aulanier et al. 2010). So, we also show the approximative results for a broad channel case, $a/D = 0.5$. For a straight current channel, the flux conservation provides an increasing stabilizing effect as the channel radius, a, is increasing (Figure 4). Indeed, for a broad straight channel ($a/D \geq 0.1$), $n_{Bp,crit.}$ can reach a value comparable, or even larger in some casesthan the one obtained for the corresponding circular channel with the same parameter values (Figure 4(e) and (f)). We conclude that the circular and straight current channels

have typically comparable instability threshold values for the range of parameters expected in the corona.

The internal evolution of the current channel during the perturbation (i.e. the effect of n_a), has a **common** effect on the stability of a circular and of a straight current channel because the stabilizing term provided by the flux conservation is generally decreased with an increase of n_a (Figures 3,4). However, changing the channel thickness (a/D) has an opposite effect on the instability threshold for a circular and for a straight current channel (compare the panels in Figure 4 where the a/D curved are ordered oppositely in the two columns). For a straight channel, $n_r = 1$, so $n_{\mathrm{Bp,crit.}} = n_r + n_I$ is affected only by the dependance of n_I on a/D. But, for a circular channel, the n_r dependance on a/D is important, and dominates the contribution of n_I, as soon as n_a is slightly positive. It implies a dependance of $n_{\mathrm{Bp,crit.}}$ on a/D for a circular channel that is opposite to that for a straight channel.

5. CONCLUSION

How to destabilize a coronal magnetic configuration is a key-issue of CME research. Among several possibilities, two candidates are a loss of equilibrium and a torus instability occuring during the evolution of the magnetic configuration. Both have been initially developed with the approximation that the coronal currents are restricted to a non-neutralized current channel, and both theory were further analyzed with MHD simulations, relaxing part of the initial approximations of the analytical developments, but at the expense of not covering the parameter space.

In this study, we revisit both analytical theories and compare their approaches for the two simple configurations where their results apparently differ: a straight and a circular current channel. A loss of equilibrium is typically, but not always, present in both configurations when an ideal-MHD evolution is imposed during the long-term evolution of the magnetic configuration. However, when a loss of equilibrium occurs, the magnetic configuration is also ideally unstable. From the results of Sections 3 and 4, we conclude that both approaches are in fact both compatible and complementary. In particular they agree on the position of instability, if no significant current sheets are formed during the long-term evolution of the magnetic configuration. Moreover, slow resistive processes, e.g. tether cutting, are probably occurring all the way before an eruption occurs. Therefore, we conclude that the analytical theory is most useful in deriving an instability threshold with the constraint of ideal MHD evolution on a short time scale (coronal Alfvén time) for a given magnetic equilibrium.

We also compare the physical origin of the instability of straight and circular current channels. In order to model the negligible evolution of the magnetic flux crossing the photosphere on the coronal Alfvén time scale, a theoretical image current is introduced below the photosphere (Figure 1). For a straight current channel, the repulsion of the image is balancing the Laplace force between the coronal current and the potential field (associated to the photospheric field distribution). For a circular current channel, the repulsion of the nearby coronal current is also present (called hoop force). However, since the repulsion force depends only on the global curvature radius and on the thickness of the current channel for a circu-

lar channel, it could lead the false conclusion that the repulsion force has a different origin for the straight and circular current channels. In fact, as shown by Garren & Chen (1994), both the coronal and the image currents generically contribute to the repulsion force of a current channel. Both terms actually combine in a single expression for a circular channel, while there is no contribution of the coronal current for a strictly straight current channel. The circular and straight current channels are simply two limits of the general case with specific properties.

The instability occurs when the potential magnetic field decreases fast enough with height, more precisely when its decay index, n_{Bp} as defined by Equation (21), is larger than a critical value $n_{\mathrm{Bp,crit.}}$. At the limit of extremely thin current channels $n_{\mathrm{Bp,crit.}} = 1$ and 1.5 for a straight and circular current channel, respectively. In fact, we show that this difference is not due to the difference in the repulsion force, but that it is due to the constraint of ideal MHD (conservation of the coronal magnetic flux below the current channel). Moreover, with the sole contribution of repulsion force to the instability threshold (i.e. $n_I = 0$ in Equation (22)), first $n_{\mathrm{Bp,crit.}} < 1$ for a circular current channel while $n_{\mathrm{Bp,crit.}} = 1$ for a straight channel, and second $n_{\mathrm{Bp,crit.}}$ approaches 1 for both circular and straight channel as the channel becomes very thin. This further indicates that there is no real difference in the origin of the repulsion force for a straight and circular current channels.

We conclude that the same physics is involved in the instability of circular and straight current channels, and that they are just two particular limiting cases of more general current paths. For the typical range of current-channel thickness expected in the coronal, and present in MHD simulations, and for a current channel expanding during an upward perturbation, $n_{\mathrm{Bp,crit.}}$ has close values for both circular and straight current channels (in the range [1.1,1.3], Figure 4(e) and (f)). If the current channel would not expand, the decay index $n_{\mathrm{Bp,crit.}}$ would be higher, typically in the range [1.2,1.5], but still not so different in both cases (Figure 4(a) and (b)). Similar critical indexes have been found in MHD simulations starting from a initial equilibrium having a coronal current channel close to half torus (Török & Kliem 2007; Schrijver et al. 2008). Otherwise, from the measurement of the height of a set of quiescent prominences, combined with potential field extrapolations, Filippov & Den (2001) found $n_{\mathrm{Bp,crit.}} \approx 1$. This threshold is closer to $n_{\mathrm{Bp,crit.}}$ of the straight current channel as expected since quiescent prominences are horizontally extended structures.

In an MHD simulation, where a flux rope and its associate current channel is progressively formed due to photospheric motions, flux cancelation, and magnetic reconnection, Aulanier et al. (2010) found an unstable configuration when $n_{\mathrm{Bp,crit.}} \approx 1.5$. There, the flux rope height satisfied $h/D \approx 1$. This was in favor of the "torus instability". However, with the above results, this threshold would require that the current channel is almost rigid during the perturbation (i.e. $n_a = 0$ as in Figure 4(b)). It is not obvious that this condition is met in a low-β magnetic field. More relevant is probably the role of the anchorage of the current channel at fixed photospheric positions during the stability analysis, a constraint not

present for both the straight and circular models studied above, but included in the non-equilibrium study of Isenberg & Forbes (2007). The present analytical theory is also over simplifying the coronal current distribution to only one current channel, while at least partial current neutralization as well as other current layers are typically present in MHD simulations. This may also raise the critical index, $n_{\mathrm{Bp,crit.}}$, to larger values (e.g. $n_{\mathrm{Bp,crit.}}$ as high as 1.9 was found in the MHD simulations of flux emergence by Fan & Gibson 2007). The precise understanding of the instability threshold is important for determining when a CME would occur. This will be the object of further developments of the analytical theory.

It would also be desirable to derive the critical index from observations of eruptive prominences and sigmoids, the pre-eruptive altitudes of which can either be measured using two vantage points (e.g. using the pair of STEREO imagers) or when they cross the solar limb.

At first approximation, the background coronal magnetic field would then have to be extrapolated in the potential field approximation, using photospheric magnetograms either taken on the same day of the eruption if possible, or a few days before if no magnetogram is available. Such a survey of various eruptive solar features would extend the work carried out by Filippov & Den (2001), who focused on long and high altitude quiescent prominences, that mostly concern the straight channel model.

REFERENCES

Aly, J. J. 1985, A&A, 143, 19
Amari, T. & Aly, J. J. 1989, A&A, 208, 261
Amari, T., Luciani, J. F., Aly, J. J., Mikic, Z., & Linker, J. 2003, ApJ, 595, 1231
Amari, T., Luciani, J. F., Mikic, Z., & Linker, J. 2000, ApJ, 529, L49
Antiochos, S. K., DeVore, C. R., & Klimchuk, J. A. 1999, ApJ, 510, 485
Anzer, U. & Ballester, J. L. 1990, A&A, 238, 365
Aulanier, G., Démoulin, P., & Grappin, R. 2005, A&A, 430, 1067
Aulanier, G., Török, T., Démoulin, P., & DeLuca, E. E. 2010, ApJ, 708, 314
Bateman, G. 1978, MHD instabilities (The Massachusetts Institute of Technology)
Chen, J. 1989, ApJ, 338, 453
Démoulin, P., Ferreira, J., & Priest, E. R. 1991, A&A, 245, 289
Démoulin, P. & Priest, E. R. 1988, A&A, 206, 336
Fan, Y. & Gibson, S. E. 2004, ApJ, 609, 1123
—. 2007, ApJ, 668, 1232
Filippov, B. P. & Den, O. G. 2001, J. Geophys. Res., 106, 25177
Forbes, T. G. 2000, J. Geophys. Res., 105, 23153
Forbes, T. G. & Isenberg, P. A. 1991, ApJ, 373, 294
Forbes, T. G., Linker, J. A., Chen, J., Cid, C., Kóta, J., Lee, M. A., Mann, G., Mikić, Z., Potgieter, M. S., Schmidt, J. M., Siscoe, G. L., Vainio, R., Antiochos, S. K., & Riley, P. 2006, Space Science Reviews, 123, 251
Forbes, T. G. & Priest, E. R. 1995, ApJ, 446, 377
Garren, D. A. & Chen, J. 1994, Physics of Plasmas, 1, 3425
Gibson, S. E., Fan, Y., Török, T., & Kliem, B. 2006, Space Science Reviews, 124, 131
Green, L. M. & Kliem, B. 2009, ApJ, 700, L83
Green, L. M., López fuentes, M. C., Mandrini, C. H., Démoulin, P., Van Driel-Gesztelyi, L., & Culhane, J. L. 2002, Sol. Phys., 208, 43
Grover, F. W. 1946, Inductance Calculations: Working Formulas and Tables (Dover Publications, Inc., New York)
Isenberg, P. A. & Forbes, T. G. 2007, ApJ, 670, 1453
Isenberg, P. A., Forbes, T. G., & Démoulin, P. 1993, ApJ, 417, 368
Jackson, J. D. 1975, Classical Electrodynamics, 2nd Edition (John Wiley & Sons, New York)
Kahler, S. W., Moore, R. L., Kane, S. R., & Zirin, H. 1988, ApJ, 328, 824
Kliem, B. & Török, T. 2006, Physical Review Letters, 96, 255002
Klimchuk, J. A. & Sturrock, P. A. 1989, ApJ, 345, 1034
Krall, J., Chen, J., & Santoro, R. 2000, ApJ, 539, 964
Kuperus, M. & Raadu, M. A. 1974, A&A, 31, 189
Lin, J., Forbes, T. G., & Isenberg, P. A. 2001, J. Geophys. Res., 106, 25053
Lin, J., Forbes, T. G., Isenberg, P. A., & Démoulin, P. 1998, ApJ, 504, 1006

Lin, J., van Ballegooijen, A. A., & Forbes, T. G. 2002, J. Geophys. Res., 107, 1438
Mackay, D. H. & van Ballegooijen, A. A. 2006, ApJ, 641, 577
Malmberg, J. H. & Rosenbluth, M. N. 1965, Review of Scientific Instruments, 36, 1886
Maričić, D., Vršnak, B., Stanger, A. L., Veronig, A. M., Temmer, M., & Roša, D. 2007, Sol. Phys., 241, 99
Martens, P. C. H. & Kuin, N. P. M. 1989, Sol. Phys., 122, 263
Moore, R. L., Larosa, T. N., & Orwig, L. E. 1995, ApJ, 438, 985
Moore, R. L. & Roumeliotis, G. 1992, in Lecture Notes in Physics, Berlin Springer Verlag, Vol. 399, IAU Colloq. 133: Eruptive Solar Flares, ed. Z. Svestka, B. V. Jackson, & M. E. Machado, 69
Neupert, W. M., Thompson, B. J., Gurman, J. B., & Plunkett, S. P. 2001, J. Geophys. Res., 106, 25215
Parker, E. N. 1996a, ApJ, 471, 489
—. 1996b, ApJ, 471, 485
Ramo, S., Whinnery, J., & Van Duzer, T. 1994, Fields and Waves in Communication Electronics,, 3rd Edition (John Wiley and Sons)
Savcheva, A. & van Ballegooijen, A. 2009, ApJ, 703, 1766
Schmieder, B., Bommier, V., Kitai, R., Matsumoto, T., Ishii, T. T., Hagino, M., Li, H., & Golub, L. 2008, Sol. Phys., 247, 321
Schrijver, C. J., Elmore, C., Kliem, B., Török, T., & Title, A. M. 2008, ApJ, 674, 586
Shafranov, V. D. 1966, Reviews of Plasma Physics, 2, 103
Temmer, M., Veronig, A. M., Vršnak, B., Rybák, J., Gömöry, P., Stoiser, S., & Maričić, D. 2008, ApJ, 673, L95
Titov, V. S. & Démoulin, P. 1999, A&A, 351, 707
Titov, V. S., Hornig, G., & Démoulin, P. 2002, J. Geophys. Res., 107(A8), 1164
Török, T. & Kliem, B. 2003, A&A, 406, 1043
—. 2005, ApJ, 630, L97
—. 2007, Astronomische Nachrichten, 328, 743
van Ballegooijen, A. A. & Martens, P. C. H. 1989, ApJ, 343, 971
van Driel-Gesztelyi, L. 1998, in Astronomical Society of the Pacific Conference Series, Vol. 155, Three-Dimensional Structure of Solar Active Regions, ed. C. E. Alissandrakis & B. Schmieder, 202–223
van Driel-Gesztelyi, L., Démoulin, P., Mandrini, C. H., Harra, L., & Klimchuk, J. A. 2003, ApJ, 586, 579
van Tend, W. & Kuperus, M. 1978, Sol. Phys., 59, 115
Venkatakrishnan, P. & Tiwari, S. K. 2009, ApJ, 706, L114
Vršnak, B. 2008, Annales Geophysicae, 26, 3089
Vršnak, B., Maričić, D., Stanger, A. L., & Veronig, A. 2004, Sol. Phys., 225, 355
Wheatland, M. S. 2000, ApJ, 532, 616
Zhang, J., Dere, K. P., Howard, R. A., Kundu, M. R., & White, S. M. 2001, ApJ, 559, 452